Rapid Communications

Observation of two sound modes in a binary superfluid gas

Joon Hyun Kim,[1] Deokhwa Hong,[1] and Y. Shin[1,2,*]

[1]*Department of Physics and Astronomy, and Institute of Applied Physics, Seoul National University, Seoul 08826, Korea*

[2]*Center for Correlated Electron Systems, Institute for Basic Science, Seoul 08826, Korea*

(Received 24 July 2019; revised manuscript received 15 April 2020; accepted 18 May 2020; published 4 June 2020)

We study the propagation of sound waves in a binary superfluid gas with two symmetric components. The binary superfluid is constituted using a Bose-Einstein condensate of ^{23}Na in an equal mixture of two hyperfine ground states. Sound waves are excited in the condensate by applying a local spin-dependent perturbation with a focused laser beam. We identify two distinct sound modes, referred to as density sound and spin sound, where the densities of the two spin components oscillate in phase and out of phase, respectively. The observed sound propagation is explained well by the two-fluid hydrodynamics of the binary superfluid. The ratio of the two sound speeds is precisely determined from a timescale analysis of the sound wave propagation, without the need of absolute density calibration, and we find it in quantitatively good agreement with the known interaction properties of the binary system.

DOI: 10.1103/PhysRevA.101.061601

Sound propagation in a superfluid is a characteristic transport phenomenon revealing the microscopic and thermodynamic properties of the superfluid system. In a long-wavelength limit, a sound wave propagates without distortion, reflecting the linear dispersion of the gapless Goldstone excitation mode of the superfluid [1]. At finite temperatures, containing a normal fluid within it, a superfluid system supports two types of sound waves, referred to as first and second sounds [2,3], and their propagation speeds are determined as functions of thermodynamic quantities such as superfluid density, entropy density, and compressibility [4]. Thus, the study of sound propagation measures our understanding of the superfluid system.

A superfluid with two superflowing components has been studied with great interest since the discovery of ^{3}He–^{4}He mixtures [5]. This interest has continued through recent experimental developments in ultracold atomic gas mixtures [6–9], exciton-polariton condensate [10], and two-gap superconductors [11]. In the binary superfluid system, interactions between two components induce the mixing of the low-energy excitation modes of each component, giving rise to two new hybridized sound waves. A peculiar aspect in the mixing is that the superflow of one component can experience a nondissipative drag from the movement of the other component [12], known as the Andreev-Bashkin (AB) effect. Such elements of mutual entrainment affect the speed of sound and can be important in the stability and robustness of the superfluidity of the binary system, particularly in a strongly interacting regime [13]. The quantitative understanding of the AB effect has been pursued in recent theoretical works [14–18], stimulating experimental efforts to measure the speed of sound in a binary superfluid system.

In this paper we investigate sound propagation in a binary superfluid gas comprised of a Bose-Einstein condensate (BEC) of ^{23}Na in an equal mixture of two hyperfine ground states. Here the two components are identical in mass, density, and intracomponent interactions. From the $\mathbb{Z}_2$ symmetry, it is expected that the superfluid shows two modes of density oscillations, i.e., sound waves, where the densities of the two components oscillate in phase and out of phase, respectively (Fig. 1). The in-phase oscillations correspond to an ordinary pressure wave whose propagation speed is determined by the compressibility of the system. Meanwhile, the out-of-phase oscillations are a wave of the density difference between the two components, which we refer to as *spin* sound, regarding the two components as two opposite spin states, $|\uparrow\rangle$ and $|\downarrow\rangle$ [19–21]. We observe two distinct sound waves propagating with different speeds in the condensate and identify the fast wave with ordinary density sound and the slow wave with spin sound. The measured propagation speeds of the two sound waves are found to be well explained by the two-fluid hydrodynamics of the binary superfluid. In particular, we

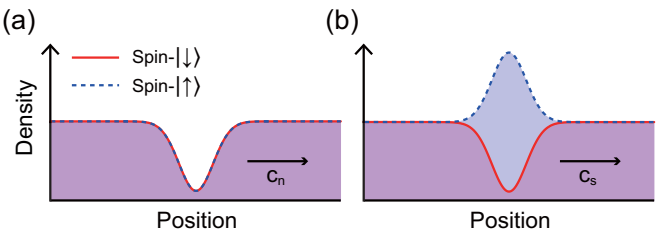

FIG. 1. Sound waves in a symmetric binary superfluid. (a) Ordinary density sound where the two superfluid components oscillate in phase, and (b) spin sound wave where they oscillate out of phase. The red solid and blue dashed lines indicate the spatial density profiles of the two components. c_n and c_s denote the propagation speeds of the density and spin sounds, respectively.

*yishin@snu.ac.kr

precisely determine the ratio of the two sound speeds from a timescale analysis of the sound wave propagation, with no need for absolute density calibration. This work establishes an experimental protocol to quantitatively study the sound propagation in a binary superfluid system.

Our experiment starts with the preparation of a BEC of ^{23}Na in the $|F = 1, m_F = 0\rangle$ hyperfine state [22]. The condensate, typically containing $\approx 3 \times 10^6$ atoms, is trapped in an optical dipole trap with trapping frequencies of $(\omega_x, \omega_y, \omega_z) = 2\pi \times (5.4, 8.0, 571)$ Hz and its Thomas-Fermi radii are $(R_x, R_y, R_z) \approx (168, 113, 1.6)\,\mu$m. A binary superfluid is realized by transferring the atoms in the $|m_F = 0\rangle$ state to a superposition of the two spin states, $|\uparrow\rangle \equiv |m_F = 1\rangle$ and $|\downarrow\rangle \equiv |m_F = -1\rangle$, by applying a short radio-frequency (rf) pulse so that the condensate comprises an equal mixture of the two spin components. The s-wave scattering lengths for the intra- and intercomponent collisions are given by $a = 54.54(20)a_0$ and $a_{\uparrow\downarrow} = 50.78(40)a_0$, respectively, with a_0 being the Bohr radius [23]. The two components are miscible for $a > a_{\uparrow\downarrow}$ [24]. To prevent the spin-exchange process generating the $|m_F = 0\rangle$ component, we tune the quadratic Zeeman energy to $q/h \approx -5.0$ Hz using microwave field dressing [25,26], and the binary superfluid is stabilized. The thermal fraction of the sample is less than 10%. The external magnetic field is $B_z = 50$ mG, and its gradient is controlled to be less than 0.1 mG/cm [27].

Sound waves are generated by applying local potential perturbations on the condensate using a focused Gaussian laser beam, as in previous works [28–31]. The laser beam penetrates along the z axis at the center of the condensate. We adiabatically turn on the laser beam by increasing its intensity over 200 ms and then rapidly switch it off in 1 ms. Sound waves are generated through the sudden change of the optical potential, and their subsequent propagation in the condensate is probed by taking absorption or spin-sensitive phase-contrast images at various hold times t after turning off the laser beam [32].

The key feature of our experiment is that the optical potential magnitudes $V^0_{\uparrow(\downarrow)}$ for the spin–$\uparrow$ ($\downarrow$) components can be differentiated by using a near-resonant laser beam. For a near-resonant laser beam, many different transition lines generating the optical dipole potential are spectroscopically resolved, so the potential ratio, $V^0_\uparrow/V^0_\downarrow$, can be controlled with the optical frequency and polarization of the laser beam [33]. In a linear regime with small optical potentials, the density $n_{\uparrow(\downarrow)}$ of the spin-$\uparrow$ ($\downarrow$) component locally varies as $g\delta n_{\uparrow(\downarrow)} + g_{\uparrow\downarrow}\delta n_{\downarrow(\uparrow)} + V^0_{\uparrow(\downarrow)} = 0$, where $g_{(\uparrow\downarrow)} = \frac{4\pi\hbar^2}{m} a_{(\uparrow\downarrow)}$, with m being the atomic mass. Then the deformations of the total density, $n = n_\uparrow + n_\downarrow$, and the spin density, $n_s = n_\uparrow - n_\downarrow$, are given by

$$\Delta n = -\frac{V^0_\uparrow + V^0_\downarrow}{g + g_{\uparrow\downarrow}} \quad \text{and} \quad \Delta n_s = -\frac{V^0_\uparrow - V^0_\downarrow}{g - g_{\uparrow\downarrow}}, \tag{1}$$

respectively. Therefore, when $V^0_\uparrow \neq V^0_\downarrow$, $\Delta n_s \neq 0$ and a spin sound wave can be generated by the local potential perturbation.

We first investigate the density perturbation with $V^0_\uparrow = V^0_\downarrow$, where we use a 532-nm far-detuned laser beam which produces identically repulsive dipole potentials for the two spin states. The $1/e^2$ intensity radius of the laser beam is 18.3(3) μm, and its potential height is approximately five times the chemical potential μ of the sample, resulting in a density-depleted hole in the condensate. In Fig. 2(a), the *in situ* density images of the sample for various hold times are displayed. We observe that a ring-shaped rarefaction pulse is generated, and it propagates out in a radial direction. During its propagation, the FWHM of the density dip is maintained at $\approx 22\,\mu$m, implying the dispersionless character of the sound wave. Performing absorption imaging after a 19-ms Stern-Gerlach (SG) spin separation [22,32], we find that both spin components show density dips at the pulse position, which indicates that the generated pulse wave is a sound wave in the in-phase oscillating mode.

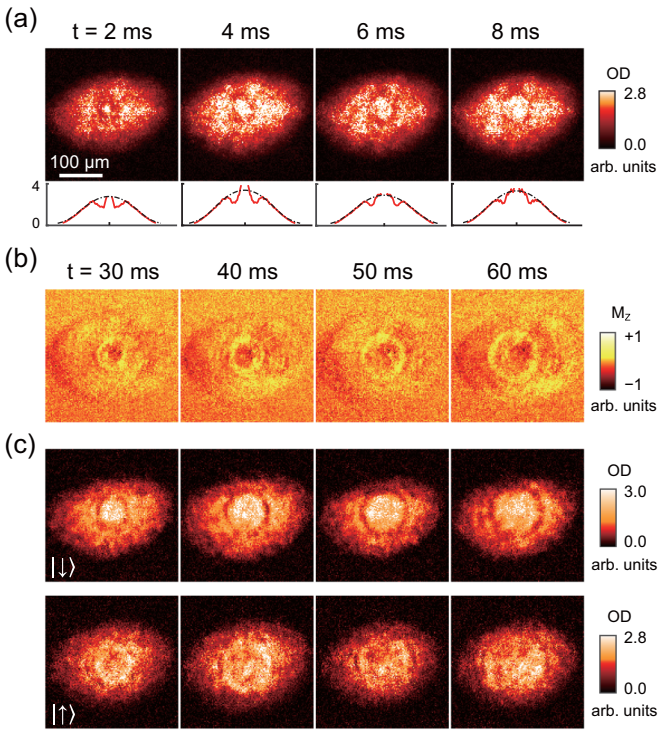

FIG. 2. Observation of the sound propagation in a binary superfluid. (a) *In situ* optical density (OD) images of the two-component Bose-Einstein condensate at various hold times t after applying a local density perturbation at the center of the condensate. A ring-shaped rarefaction pulse is generated, and it propagates outwardly. The bottom row shows the averaged radial profiles obtained from the images. The dash-dotted line is a guide for an unperturbed sample. (b) *In situ* magnetization (M_z) images of the condensate at various t after applying a local spin perturbation and (c) the corresponding OD images of the two spin components taken after a 19-ms time of flight with Stern-Gerlach (SG) spin separation. The spin-$\downarrow$ component shows a density dip and the spin-$\uparrow$ component a density lump at wave pulse position.

Next, we investigate the sound wave generation by spin-dependent perturbation with $V^0_\uparrow = -V^0_\downarrow$, where we employ a 589-nm near-resonant laser beam. To generate asymmetric potentials for the two spin states, we tune the optical frequency of the laser beam at $2\pi \times 508.505$ THz between the $D1$ and $D2$ lines of ^{23}Na and set its polarization to be σ^-, resulting in attractive and repulsive potentials for the spin–$\uparrow$

and ↓ components [33]. The $1/e^2$ radius of the beam is 11(1) μm and its potential magnitude is $V^0_{\uparrow(\downarrow)} \approx \mp 1.1\mu$.

Figure 2(b) shows the *in situ* magnetization images of the sample for various hold times after turning off the 589-nm laser beam [8]. A ring-shaped pulse wave carrying a positive magnetization is observed as propagating out from the center of the condensate. It is noticeable that the magnetization pulse propagates much more slowly than the density wave presented in the previous case, indicating that it is a different type of sound wave. The FWHM of the magnetization pulse is initially $\approx 9\,\mu$m and increases to $\approx 14\,\mu$m after 60 ms propagation. From the absorption images taken after SG spin separation, we observe that the spin–↓ component shows a density dip at the position of the propagating pulse wave, whereas the spin–↑ component shows a density lump at the same position [Fig. 2(c)]. This clearly demonstrates the generation of a spin sound wave in the binary superfluid system.

In the spin sound generation experiment, the magnitude of the asymmetric optical potential is high so that the spin-↓ component is locally depleted in the perturbing region, whereas the spin-↑ component is increased to have $\Delta n \approx \frac{\mu}{g} \neq 0$. This means that a density sound wave might be also generated with the strong spin-dependent perturbation. When $|V^0_\uparrow - V^0_\downarrow| > 2\frac{g-g_{\uparrow\downarrow}}{g+g_{\uparrow\downarrow}}\mu \approx 0.1\mu$, the perturbing region becomes fully spin-polarized and the asymmetric potential induces a total density deformation. In our *in situ* measurement of sound propagation, we employed strong perturbations to clearly locate the position of the pulse wave. It was experimentally checked using absorption imaging with SG spin separation that no systematic effect on the sound propagation speed arises from the strong perturbations.

In a long-wavelength limit, zero-temperature dynamics of a binary superfluid is well described by two-fluid hydrodynamic equations [21]:

$$\partial_t n_i + \nabla \cdot (n_i \boldsymbol{u}_i) = 0,$$
$$\partial_t \boldsymbol{u}_i + \nabla\left(\frac{1}{2}u_i^2 + \frac{g}{m}n_i + \frac{g_{\uparrow\downarrow}}{m}n_j\right) = 0, \qquad (2)$$

where $\boldsymbol{u}_{i(j)}$ is the velocity of the spin-$i(j)$ component ($i, j = \uparrow, \downarrow$ and $i \neq j$). The first equation is the continuity equation, and the second is the Euler equation with the chemical potential of the spin-i component, $\mu_i = gn_i + g_{\uparrow\downarrow}n_j$. By linearizing the equations for a stationary state with $\boldsymbol{u}_{\uparrow(\downarrow)} = 0$ and finding the condition to have a traveling wave solution of $\delta n_i = A_i \sin(\boldsymbol{k}\cdot\boldsymbol{r} - \omega t)$, we obtain the wave velocity $v_s = \omega/k$ as

$$v^2_{s\pm} = \frac{1}{2m}\left[gn \pm \sqrt{g^2_{\uparrow\downarrow}n^2 + (g^2 - g^2_{\uparrow\downarrow})n_s^2}\right]. \qquad (3)$$

For $g > g_{\uparrow\downarrow} > 0$, there are always two sound modes with different propagation speeds.

In a symmetric binary superfluid with $n_s = 0$, the two sound velocities are given by $v_{s\pm} = \sqrt{\frac{1}{2m}(g \pm g_{\uparrow\downarrow})n}$. The fast wave is density sound for $A_\uparrow = A_\downarrow$ and the slow wave is spin sound for $A_\uparrow = -A_\downarrow$, which is consistent with our experimental observations. The mass current $\boldsymbol{j}_m = n_\uparrow \boldsymbol{u}_\uparrow + n_\downarrow \boldsymbol{u}_\downarrow$ and spin current $\boldsymbol{j}_s = n_\uparrow \boldsymbol{u}_\uparrow - n_\downarrow \boldsymbol{u}_\downarrow$ are decoupled in the superfluid, which reflects a peculiar consequence of the $\mathbb{Z}_2$ symmetry of the binary system, and the Bogoliubov quasiparticles are thus given by pure phonons and magnons [34]. Our observation of the spin sound propagation demonstrates the existence of the gapless magnon mode associated with the relative phase of the two spin components and corroborates the spin superfluidity of the binary system [35–37].

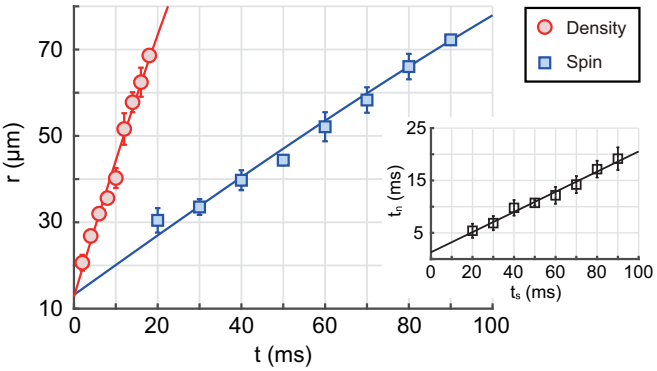

FIG. 3. Time evolution of the radius of the ring-shaped wave pulse, r_n (red circles) for the density sound wave and r_s (blue squares) for the spin sound wave. Each data point consists of five measurements of the same experiment and its error bar indicates their standard deviation. The solid lines are the model curves of $r(t) = R\sin(ct/R + \theta_0)$, fitted to the experimental data, where R is the condensate radius, c is the speed of sound at the sample center, and $R\sin(\theta_0)$ is the initial position of the sound wave. The inset shows the constructed data $\{t_s, t_n\}$ for the timescale analysis of the sound wave propagation (see text for details). The error bar of each data point shows the uncertainty from its determination using linear interpolation, and the solid line is a linear function fit to the data.

We measure the sound propagation speed from the time evolution of the radius r of the ring-shaped pulse wave (Fig. 3). The averaged radial profile is obtained from the *in situ* image, and r is determined with the radial position for the local density minimum (magnetization maximum) of the pulse wave for the density (spin) sound. Taking into account the inhomogeneous density profile of the trapped sample, we model the radial dependence of the propagation speed as $v_r(r) = c\sqrt{1 - r^2/R^2}$, with the peak speed c at the sample center and $R = \sqrt{R_x R_y}$, and obtain a model function of $r(t) = R\sin(ct/R + \theta_0)$ for the ring radius by integrating $v_r(r)$ over time. From the model function fit to the experimental data, we determine the speed c and the initial position $r(0) = R\sin(\theta_0)$ of the sound wave. In our measurements, the sound velocities are given by $c_n = 3.23(18)$ mm/s for density sound and $c_s = 0.70(4)$ mm/s for spin sound, which are found to be in agreement with the estimations of $v_{s+} = 3.22(5)$ mm/s and $v_{s-} = 0.61(4)$ mm/s from Eq. (3). In the calculation of $v_{s\pm}$, we use the effective density $n = (2/3)n_0$, with n_0 being the peak density of the condensate, under the assumption of the hydrodynamics equilibrium along the tight confining z direction of the highly oblate sample [38–41]. The initial positions $r_{n(s)}(0)$ of the sound waves are measured to be $\approx 13\,\mu$m, which are comparable to the spatial sizes of the used laser beams.

Here we remark that, although the individual velocities of c_n and c_s depend on the details of the sample condition such as the particle density and the trapping geometry, the ratio

$\gamma = c_s/c_n$ is a quantity that faithfully reflects the intrinsic properties of the binary superfluid because both velocities have the same density dependence. The measurement results of c_n and c_s give $\gamma = 0.217(17)$. However, we find that γ can be directly measured by a timescale analysis of the two experimental data sets for the density and spin sound waves, which requires no assumption concerning the density profile of the sample. We perform the scale analysis as follows: For each data point $\{t_s, r_s\}$ in the spin sound measurement we determine the corresponding time t_n for the density sound wave to have the same radius $r_n = r_s$ using linear interpolation of the density sound measurement data. We then obtain γ by fitting a linear function $t_n = \gamma t_s + \beta$ to the constructed data $\{t_s, t_n\}$ (Fig. 3, inset). Here the offset β accounts for the difference of the initial positions of the two sound waves. In the scale analysis, we obtain $\gamma = 0.193(22)$, which is in quantitatively good agreement with the predicted value of $\gamma_0 = \frac{v_{s-}}{v_{s+}} = \sqrt{\frac{a-a_{\uparrow\downarrow}}{a+a_{\uparrow\downarrow}}} = 0.189(11)$.

Because the timescale analysis of the two sound waves is free from systematic errors associated with absolute density calibration, the measurement of γ can be a powerful method for probing the subtle interaction effects in binary superfluid systems. In Ref. [15] it was shown that the AB entrainment effect modifies only the speed of spin sound, not density sound, thus resulting in a direct shift in γ. In our weakly interacting system with $n_0 a^3 \approx 1.4 \times 10^{-6}$, the fractional weight of the superfluid drag is predicted to be $\approx 4 \times 10^{-4}$ [14], and the corresponding shift in γ is too small to be resolved for the current uncertainties of the scattering lengths, a and $a_{\uparrow\downarrow}$ [23]. The precise measurement of γ with strongly interacting systems would provide an interesting opportunity to observe the AB effect [15,17]. It should be noted that the Lee-Huang-Yang (LHY) corrections arising from quantum fluctuations also can cause a shift in γ. In our sample, for instance, the relative shift of c_n due to the LHY corrections is estimated to be about 0.5% [42], which is one order of magnitude larger than that of c_s due to the AB effect. Therefore, the LHY corrections need to be taken into account for a quantitative understanding of γ.

Finally, we explore the general case of $|V_\uparrow^0| \neq |V_\downarrow^0|$, where both density and spin sound waves would be generated simultaneously. In Fig. 4, we display density and magnetization images of the sample that is perturbed with $V_\uparrow^0 \approx -3\mu$ and $V_\downarrow^0 \approx \mu$. The images were taken with a 19-ms time of flight to enhance the detection of sound waves. It is clearly shown that both density and spin sound waves are generated but propagate separately in the condensate, highlighting their different speeds. The density wave appears as a density lump because $V_\uparrow^0 + V_\downarrow^0 < 0$, and the spin sound wave carries positive magnetization because $V_\uparrow^0 - V_\downarrow^0 < 0$.

A notable observation is that a solitonlike magnetized object is created together with the two sound waves (Fig. 4, lower row). The magnetized object moves slower than the spin wave, with preserving its spatial size and shape. We interpret

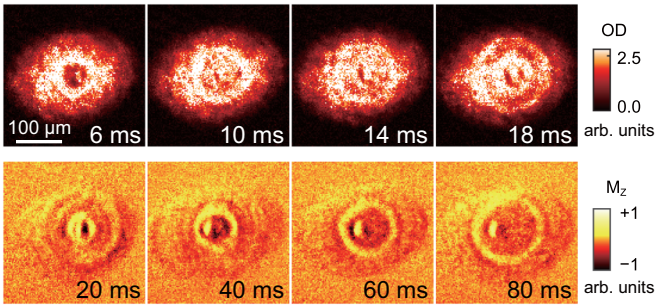

FIG. 4. Simultaneous generation of density and spin sound waves with strong spin-dependent perturbation. OD images (upper row) and magnetization images (lower row) for various hold times, taken with a 19-ms time of flight. A fast density wave and a slow spin wave propagate radially from the center. A solitonic object with a magnetized core is created together with the two sound waves, moving slower than the spin wave.

it as a small dipole of half-quantum vortices (HQVs) with the same core magnetization, which explains the bending shape of the object and its linear motion [43]. HQVs are the defects involving both mass and spin circulations, so their creation reveals that there was nonlinear coupling between mass and spin currents in the sound wave generation via the strong spin-dependent perturbation. The dipole's moving velocity of $\approx c_s/2$ suggests that the separation between the two HQVs is $\approx 2\xi_s$, where ξ_s is the spin healing length, implying that their magnetized cores are almost coalesced [8]. In the experiment, the generation of the solitonic object was near deterministic, and we reason that it must be due to the asymmetric shape of the optical potential.

In conclusion, we have investigated sound propagation in the symmetric binary superfluid and observed two distinct sound modes in density and spin channels, respectively. The ratio γ of the two sound velocities was precisely measured from a timescale analysis without absolute density calibration. An interesting extension of this work would be to investigate the temperature dependence of γ and its evolution in the dimensional crossover to two and one dimension (Refs. [16,17], respectively). In particular, in our highly oblate sample, the density and spin healing lengths, ξ_n and ξ_s, respectively, give a length hierarchy such that $\xi_n < R_z < \xi_s$. Thus, thermal effects might have different dimensional characteristics for the density and spin channels, possibly resulting in a variation of γ. We also expect that the spin-dependent potential of the near-resonant laser beam can be extensively used to investigate the dynamics of various topological objects in the spinor superfluid, such as HQVs [8,43], skyrmions or merons [22], and magnetic solitons [44].

This work was supported by the Samsung Science and Technology Foundation (Project No. SSTF-BA1601-06) and the National Research Foundation of Korea (Grant No. NRF-2018-2018R1A2B3003373).

[1] L. D. Landau, Theory of the superfluidity of helium II, Phys. Rev. **60**, 356 (1941).

[2] C. T. Lane, H. A. Fairbank, and W. M. Fairbank, Second sound in liquid helium II, Phys. Rev. **71**, 600 (1947).

[3] L. A. Sidorenkov, M. K. Tey, R. Grimm, Y.-H. Hou, L. Pitaevskii, and S. Stringari, Second sound and the superfluid fraction in a Fermi gas with resonant interactions, Nature (London) **498**, 78 (2013).

[4] T. D. Lee and C. N. Yang, Low-temperature behavior of a dilute Bose system of hard spheres, II. Nonequilibrium properties, Phys. Rev. **113**, 1406 (1959).

[5] D. O. Edwards, D. F. Brewer, P. Seligman, M. Skertic, and M. Yaqub, Solubility of He^3 in Liquid He^4 at 0 K, Phys. Rev. Lett. **15**, 773 (1965).

[6] G. Modugno, M. Modugno, F. Riboli, G. Roati, and M. Inguscio, Two Atomic Species Superfluid, Phys. Rev. Lett. **89**, 190404 (2002).

[7] M. Delehaye, S. Laurent, I. Ferrier-Barbut, S. Jin, F. Chevy, and C. Salomon, Critical Velocity and Dissipation of an Ultracold Bose-Fermi Counterflow, Phys. Rev. Lett. **115**, 265303 (2015).

[8] S. W. Seo, S. Kang, W. J. Kwon, and Y. Shin, Half-Quantum Vortices in an Antiferromagnetic Spinor Bose-Einstein Condensate, Phys. Rev. Lett. **115**, 015301 (2015).

[9] C. R. Cabrera, L. Tanzi, J. Sanz, B. Naylor, P. Thomas, P. Cheiney, and L. Tarruell, Quantum liquid droplets in a mixture of Bose-Einstein condensates, Science **359**, 301 (2018).

[10] K. G. Lagoudakis, T. Ostatnický, A. V. Kavokin, Y. G. Rubo, R. André, and B. Deveaud-Plédran, Observation of half-quantum vortices in an exciton-polariton condensate, Science **326**, 974 (2009).

[11] M. Zehetmayer, A review of two-band superconductivity: Materials and effects on the thermodynamic and reversible mixed-state properties, Supercond. Sci. Technol. **26**, 043001 (2013).

[12] A. F. Andreev and E. P. Bashkin, Three-velocity hydrodynamics of superfluid solutions, Zh. Eksp. Teor. Fiz. **69**, 319 (1975) [Sov. Phys.-JETP **42**, 164 (1975)].

[13] D. N. Kobyakov and C. J. Pethick, Two-component superfluid hydrodynamics of neutron star cores, Astrophys. J. **836**, 203 (2017).

[14] D. V. Fil and S. I. Shevchenko, Nondissipative drag of superflow in a two-component Bose gas, Phys. Rev. A **72**, 013616 (2005).

[15] J. Nespolo, G. E. Astrakharchik, and A. Recati, Andreev-Bashkin effect in superfluid cold gases mixtures, New J. Phys. **19**, 125005 (2017).

[16] O. I. Utesov, M. I. Baglay, and S. V. Andreev, Effective interactions in a quantum Bose-Bose mixture, Phys. Rev. A **97**, 053617 (2018).

[17] L. Parisi, G. E. Astrakharchik, and S. Giorgini, Spin Dynamics and Andreev-Bashkin Effect in Mixtures of One-Dimensional Bose Gases, Phys. Rev. Lett. **121**, 025302 (2018).

[18] V. Karle, N. Defenu, and T. Enss, Coupled superfluidity of binary Bose mixtures in two dimensions, Phys. Rev. A **99**, 063627 (2019).

[19] A. M. Kamchatnov, Y. V. Kartashov, P.-É. Larré, and N. Pavloff, Nonlinear polarization waves in a two-component Bose-Einstein condensate, Phys. Rev. A **89**, 033618 (2014).

[20] Y. Li, C. Qu, Y. Zhang, and C. Zhang, Dynamical spin-density waves in a spin-orbit-coupled Bose-Einstein condensate, Phys. Rev. A **92**, 013635 (2015).

[21] S. K. Ivanov and A. M. Kamchatnov, Simple waves in a two-component Bose-Einstein condensate, Phys. Rev. E **97**, 042208 (2018).

[22] J. Choi, W. J. Kwon, and Y. Shin, Observation of Topologically Stable 2D Skyrmions in an Antiferromagnetic Spinor Bose-Einstein Condensate, Phys. Rev. Lett. **108**, 035301 (2012).

[23] S. Knoop, T. Schuster, R. Scelle, A. Trautmann, J. Appmeier, and M. K. Oberthaler, Feshbach spectroscopy and analysis of the interaction potentials of ultracold sodium, Phys. Rev. A **83**, 042704 (2011).

[24] J. Stenger, S. Inouye, D. M. Stamper-Kurn, H.-J. Miesner, A. P. Chikkatur, and W. Ketterle, Spin domains in ground-state Bose-Einstein condensates, Nature (London) **396**, 345 (1998).

[25] F. Gerbier, A. Widera, S. Fölling, O. Mandel, and I. Bloch, Resonant control of spin dynamics in ultracold quantum gases by microwave dressing, Phys. Rev. A **73**, 041602(R) (2006).

[26] L. Zhao, J. Jiang, T. Tang, M. Webb, and Y. Liu, Dynamics in spinor condensates tuned by a microwave dressing field, Phys. Rev. A **89**, 023608 (2014).

[27] J. H. Kim, D. H. Hong, S. Kang, and Y. Shin, Metastable hard-axis polar state of a spinor Bose-Einstein condensate under a magnetic field gradient, Phys. Rev. A **99**, 023606 (2019).

[28] M. R. Andrews, D. M. Kurn, H.-J. Miesner, D. S. Durfee, C. G. Townsend, S. Inouye, and W. Ketterle, Propagation of Sound in a Bose-Einstein Condensate, Phys. Rev. Lett. **79**, 553 (1997).

[29] J. Joseph, B. Clancy, L. Luo, J. Kinast, A. Turlapov, and J. E. Thomas, Measurement of Sound Velocity in a Fermi Gas near a Feshbach Resonance, Phys. Rev. Lett. **98**, 170401 (2007).

[30] R. Meppelink, S. B. Koller, and P. van der Straten, Sound propagation in a Bose-Einstein condensate at finite temperatures, Phys. Rev. A **80**, 043605 (2009).

[31] J. L. Ville, R. Saint-Jalm, É. Le Cerf, M. Aidelsburger, S. Nascimbène, J. Dalibard, and J. Beugnon, Sound Propagation in a Uniform Superfluid Two-Dimensional Bose Gas, Phys. Rev. Lett. **121**, 145301 (2018).

[32] S. W. Seo, Dynamics of half-quantum vortices in a spinor Bose-Einstein condensate, PhD thesis, Seoul National University, 2017.

[33] R. Grimm, M. Weidemüller, and Y. B. Ovchinnikov, Optical dipole traps for neutral atoms, Adv. At. Mol. Opt. Phys. **42**, 95 (2000).

[34] Y. Kawaguchi and M. Ueda, Spinor Bose-Einstein condensates, Phys. Rep. **520**, 253 (2012).

[35] H. Flayac, H. Terças, D. D. Solnyshkov, and G. Malpuech, Superfluidity of spinor Bose-Einstein condensates, Phys. Rev. B **88**, 184503 (2013).

[36] J. H. Kim, S. W. Seo, and Y. Shin, Critical Spin Superflow in a Spinor Bose-Einstein Condensate, Phys. Rev. Lett. **119**, 185302 (2017).

[37] E. Fava, T. Bienaimé, C. Mordini, G. Colzi, C. Qu, S. Stringari, G. Lamporesi, and G. Ferrari, Observation of Spin Superfluidity in a Bose Gas Mixture, Phys. Rev. Lett. **120**, 170401 (2018).

[38] E. Zaremba, Sound propagation in a cylindrical Bose-condensed gas, Phys. Rev. A **57**, 518 (1998).

[39] S. Stringari, Dynamics of Bose-Einstein condensed gases in highly deformed traps, Phys. Rev. A **58**, 2385 (1998).

[40] W. Weimer, K. Morgener, V. P. Singh, J. Siegl, K. Hueck, N. Luick, L. Mathey, and H. Moritz, Critical Velocity in the BEC-BCS Crossover, Phys. Rev. Lett. **114**, 095301 (2015).

[41] J. W. Park, B. Ko, and Y. Shin, Critical Vortex Shedding in a Strongly Interacting Fermionic Superfluid, Phys. Rev. Lett. **121**, 225301 (2018).

[42] S. Uchino, M. Kobayashi, and M. Ueda, Bogoliubov theory and Lee-Huang-Yang corrections in spin-1 and spin-2 Bose-Einstein condensates in the presence of the quadratic Zeeman effect, Phys. Rev. A **81**, 063632 (2010).

[43] S. W. Seo, W. J. Kwon, S. Kang, and Y. Shin, Collisional Dynamics of Half-Quantum Vortices in a Spinor Bose-Einstein Condensate, Phys. Rev. Lett. **116**, 185301 (2016).

[44] C. Qu, L. P. Pitaevskii, and S. Stringari, Magnetic Solitons in a Binary Bose-Einstein Condensate, Phys. Rev. Lett. **116**, 160402 (2016).